ACADEMIC PRESS

Available online at www.sciencedirect.com
SCIENCE DIRECT®

Journal of Catalysis 215 (2003) 245–253

JOURNAL OF CATALYSIS

www.elsevier.com/locate/jcat

Adsorption and bonding of 2-butenal on Sn/Pt surface alloys

E. Janin, H. von Schenck, S. Ringler, J. Weissenrieder, T. Åkermark, and M. Göthelid *

Material och halvledarfysik, IMIT, KTH, Electrum 229, 164 40 Kista, Sweden

Received 2 September 2002; revised 16 December 2002; accepted 18 December 2002

Abstract

The adsorption of 2-butenal on the Pt(111), Pt(111)Sn-(2 × 2), and Pt(111)Sn-($\sqrt{3} \times \sqrt{3}$)R30° surfaces has been studied by high-resolution photoelectron spectroscopy and DFT calculations. On Pt(111) 2-butenal adsorbs at a threefold hollow in a η_3(C,C,O) configuration. A similar geometry is observed for Pt(111)Sn-(2×2), although the oxygen coordinates to tin instead of platinum. As the surface coverage of tin increases, as for Pt(111)Sn-($\sqrt{3} \times \sqrt{3}$)R30°, the most stable adsorption geometry changes to η_1(O), where the carbonyl oxygen once again coordinates to tin. The carbonyl bond thus retains an activated character as Pt/Sn alloys are formed. The alkene/surface interaction is, however, dramatically influenced at increasing surface concentrations of tin.

Keywords: Photoelectron spectroscopy; DFT; Chemisorption; Unsaturated aldehydes; Platinum; Low-index single-crystal surfaces

1. Introduction

The hydrogenation of α,β-unsaturated aldehydes puts the focus on challenging selectivity issues. Due to the presence of two unsaturated bonds (C=C and C=O), three types of products can be obtained, i.e., the unsaturated alcohol (hydrogenation of the C=O bond), the saturated aldehyde (hydrogenation of the C=C bond), and the saturated alcohol (hydrogenation of both bonds). The unsaturated alcohols are desirable hydrogenation products, being in turn reactants in the fine chemicals industry [1–3]. However, since thermodynamics favors hydrogenation of the alkene bond over the carbonyl, saturated aldehydes are often the dominating products [4,5]. In order to control the selectivity it is necessary to determine which parameters that influence the hydrogenation toward one product or the other. Several factors are known to play a crucial roles in this regard, e.g., the catalyst metal [6–8], the orientation of the surface [6,9–11], the presence of promoters, e.g., Sn [11], Ge [12], or Fe [13]. Moreover, different substituents at the β-carbon can have a significant impact on alkene bond activation [6,7,13].

In this paper, we have compared the behavior of 2-butenal (crotonaldehyde) on Pt(111) and on tin-modified Pt(111) surfaces, tin being an additive known to enhance the selectivity for the unsaturated alcohol. The geometry of tin-modified Pt single-crystal surfaces has been studied extensively [14–19]. Formation of surface alloys displaying single-layer characteristics has been observed at certain coverage's and annealing temperatures. Models for two surface alloys have been proposed by Paffett and Windham [14]. The Pt(111)Sn-(2 × 2) surface alloy is found at 0.25 ML (monolayers) of tin and the Pt(111)Sn-($\sqrt{3} \times \sqrt{3}$)R30° at 0.33 ML of tin. These surface alloys will henceforth be referred to as (2 × 2) and ($\sqrt{3} \times \sqrt{3}$), respectively. Schematic representations of the surface alloys are given in Fig. 1. In order to compensate for the different size of the tin and platinum atoms both surfaces are buckled, with an outward displacement of the Sn atoms by 0.30 and 0.22 Å for the (2 × 2) and the ($\sqrt{3} \times \sqrt{3}$) surface alloys, respectively [17].

Adsorption of molecules has been studied on these surfaces, ranging from O_2, H_2, and CO [20–22] to more complex molecules such as alkenes (C_2H_4, C_3H_6, C_4H_8) [23,24] and alcohols [25]. For these latter molecules, the incorporation of Sn in the topmost layer of the Pt(111) surface does not have any measurable effect on the initial sticking coefficient at low temperature, nor on the saturation coverage, but a decrease of the adsorption energy is observed [24,25]. In previous work, the adsorption of propene and 2-butenal on Pt(111) was studied by high-resolution photoelectron spectroscopy (PES) and the involvement of the carbonyl group in the bonding to the surface was evidenced [26]. The present

* Corresponding author.
E-mail address: gothelid@imit.kth.se (M. Göthelid).

0021-9517/03/$ – see front matter
doi:10.1016/S0021-9517(03)00016-2

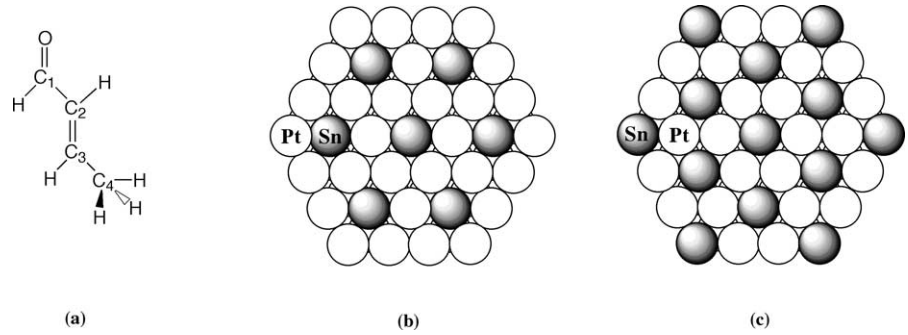

Fig. 1. (a) Schematic representation of 2-butenal, (b) Pt(111)Sn-(2 × 2), and (c) Pt(111)Sn-($\sqrt{3} \times \sqrt{3}$)R30°.

Table 1
Fitting parameters used for the Pt $4f_{7/2}$ and Sn $4d_{5/2}$ core levels

	Pt $4f_{7/2}$									Sn $4d_{5/2}$					
	B			S_1			S_2			P_1			P_2		
	Γ_L	Γ_G	α	Γ_L	Γ_G	α	Γ_L	Γ_G	α	Γ_L	Γ_G	α	Γ_L	Γ_G	α
(1 × 1)/clean	0.43	0.16	0.1	0.25	0.16	0.1	–	–	–	–	–	–	–	–	–
(1 × 1)/butenal	0.43	0.16	0.1	0.25	0.16	0.1	0.25	0.26	0.07	–	–	–	–	–	–
(2 × 2)/butenal	0.43	0.16	0.1	0.25	0.16	0	0.25	0.26	0	0.10	0.13	0	0.10	0.24	0
($\sqrt{3} \times \sqrt{3}$)/butenal	0.43	0.1	0.07	0.25	0.10	0	0.25	0.26	0	0.10	0.11	0	0.10	0.18	0

B, S_1, and S_2 represent bulk, clean surface, and adsorbate covered contributions, respectively. Γ_L and Γ_G are the Lorentzian and Gaussian widths (eV), respectively, and α is the singularity parameter.

work focuses on the influence of Sn on the bonding configuration of the molecule.

2. Photoelectron spectroscopy

2.1. Experimental procedure

The experiments were performed at beam line I511, Maxlab, in Lund, Sweden [27]. This beam line is an undulator-based VUV, soft X-ray beam line using a modified SX-700 monochromator. The photoemission spectra were recorded in normal emission at 100 K with a rotable Scienta SES200 electron spectrometer [28]. Connected to the photoemission chamber is a preparation chamber equipped with sputtering facilities, and low-energy electron diffraction (LEED) optics as well as sample heating and liquid nitrogen cooling possibilities. Temperatures were measured with a chromel-alumel thermocouple spot-welded on the side of the sample. The Pt(111) surface was prepared by argon sputtering and oxygen treatment at high temperature (800 K), followed by flashing to 1100 K in order to obtain a smooth surface. The surface alloys were prepared by evaporation of Sn (Alfa products, m5N) from a tungsten filament evaporator. Excellent LEED patterns, (2 × 2) or ($\sqrt{3} \times \sqrt{3}$)R30°, were obtained after deposition of 0.25 or 0.33 ML of tin, followed by annealing to 850 K for 1 min. The 2-butenal (Aldrich, 99+%) was purified prior to use by several freeze-pump-thaw cycles and was dosed onto the sample via a "pulse" leak valve (5 ms width pulses) in the preparation chamber. The surface was reprepared before each exposure in order to minimize CO contamination and beam-damage problems. No ordered overlayers were observed by LEED. The energy resolution was 30–50 meV for both the Pt $4f_{7/2}$ and Sn 4d spectra, and approximately 80 meV for the C 1s spectra.

2.2. Data analysis

The obtained Pt $4f_{7/2}$ core-level spectra were fitted using the number of peaks expected for the different phases; bulk (B), clean surface (S_1), and adsorbate covered surface (S_2). An asymmetric Voigt line profile was used to describe the core-level line shape [29]. The fitting parameters determining the shape of the components are thus the Lorentzian width Γ_L, the Gaussian width Γ_G and the asymmetry parameter, or singularity α. Γ_L is obtained from the clean surface spectrum for the bulk and the surface components and kept constant independently of the surface preparation. Γ_G and α are allowed to vary in the spectra obtained after Sn deposition or molecule adsorption. Two components are observed in the Sn $4d_{5/2}$ core-level spectra upon 2-butenal adsorption (P_1 and P_2). All fitting parameters are summarized in Table 1. Binding energies and relative intensities are given in Table 2. All binding energies are measured relative to the Fermi level of the Pt crystal.

2.3. Results

The Pt $4f_{7/2}$ spectrum obtained at 125 eV photon energy on the Pt(111) surface (referred to as (1 × 1)) is displayed at the bottom of Fig. 2a. A bulk and a surface contribution labeled B and S_1, respectively, can be extracted by the

Table 2
Summary of the binding energies and intensities in the Pt $4f_{7/2}$ and Sn $4d_{5/2}$ core levels

2-Butenal		Pt $4f_{7/2}$								Sn $4d_{5/2}$		
Surface	Dose	B		S_1			S_2			P_1	P_2	
		E_B	I (%)	E_B	ΔE	I (%)	E_B	ΔE	I (%)	E_B	E_B	I_2 (%)
(1×1)	0	70.86	41	70.49	−0.37	59	–	–	–	–	–	–
	40	70.88	55	70.54	−0.34	8	71.18	0.30	33	–	–	–
(2×2)	0	70.84	47	70.63	−0.21	53	–	–	–	24.13	–	–
	40	70.89	55	70.75	−0.14	10	71.32	0.43	32	24.19	24.33	53
$(\sqrt{3} \times \sqrt{3})$	0	70.84	51	70.61	−0.23	49	–	–	–	24.16	–	–
	40	70.86	66	70.69	−0.17	23	71.34	0.48	9	24.18	24.28	65

B, S_1, and S_2 represent bulk, clean surface, and adsorbate-covered contributions, respectively. E_B is the binding energy (eV), ΔE is the core-level shift compared to the bulk contribution (eV), and I (%) is the relative intensity.

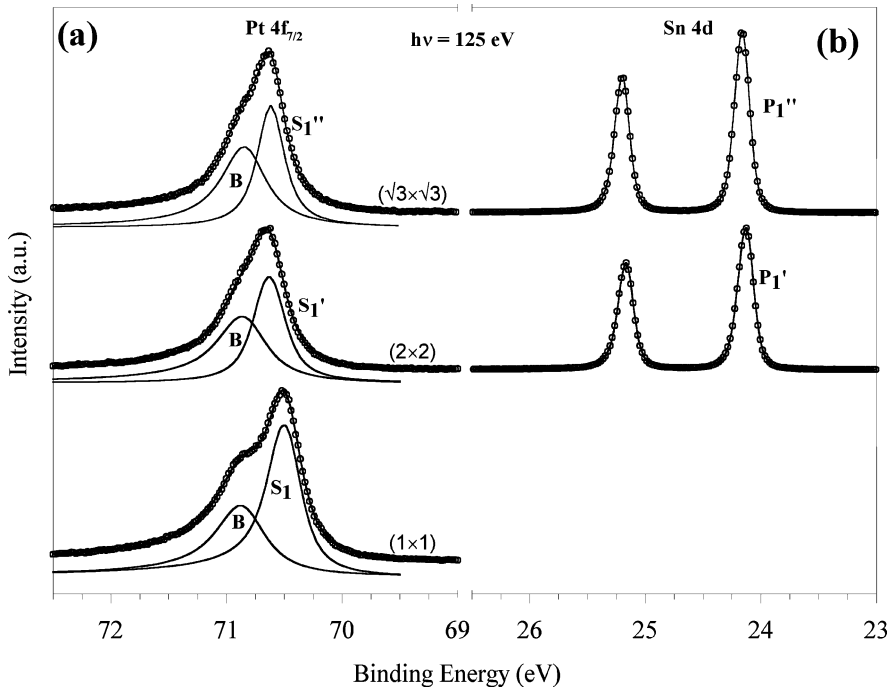

Fig. 2. (a) Core-level spectra of Pt $4f_{7/2}$ and (b) Sn 4d recorded at 125 eV photon energy for Pt(111), Pt(111)Sn-(2×2), and Pt(111)Sn-$(\sqrt{3} \times \sqrt{3})$R30°.

fitting procedure described above. The surface shift, equal to −0.37 eV, and the relative intensities (41/59%) are in good agreement with previously published data [22]. After deposition of tin and subsequent annealing, two LEED patterns are obtained depending on the initial Sn coverage, i.e., a (2×2) and a $(\sqrt{3} \times \sqrt{3})$R30° pattern. The corresponding Pt $4f_{7/2}$ core-level spectra are presented in the middle and upper part of Fig. 2a. The line shapes are very similar for the two alloys and can be fitted using two components, B and S_1' (S_1''). The surface core-level shift observed for the $(\sqrt{3} \times \sqrt{3})$ is 0.23 eV, similar to previously reported shifts [22]. The shift measured for the (2×2) surface is 0.21 eV. The corresponding Sn 4d core-level spectra are presented in Fig. 2b. A single component, P_1, appears at 24.13 and 24.16 eV for the (2×2) and $(\sqrt{3} \times \sqrt{3})$ surfaces, respectively. The binding energy obtained for the $(\sqrt{3} \times \sqrt{3})$ alloy is in accord with the literature [22]. The fact that the Sn $4d_{5/2}$ levels appear at the same binding energy for both surface alloys is not so surprising, since the Sn atoms have the same number of neighboring Pt atoms.

The three surfaces were exposed to a series of doses of 2-butenal, namely 10, 20, and 40 pulses (20 pulses corresponding to approximately 1 ML coverage on the clean Pt(111) surface). Considering again the Pt $4f_{7/2}$ and Sn $4d_{5/2}$ core-level spectra, a similar behavior was observed for the three surfaces. For clarity, only the spectra obtained after a dose of 40 pulses are presented in Fig. 3. In the Pt $4f_{7/2}$ spectra, new adsorbate-induced components labeled S_2, S_2', and S_2'' appear on the high binding energy side, with chemical shifts of 0.30 (S_2), 0.43 (S_2'), and 0.48 eV (S_2'') compared to the bulk component for the (1×1), the (2×2), and the $(\sqrt{3} \times \sqrt{3})$ surfaces, respectively. The binding energy of this adsorbate-shifted component remains stable through the entire range of exposure. This is also true for S_1, the clean surface-shifted component on Pt(111). In contrast, the clean surface components on the (2×2) and

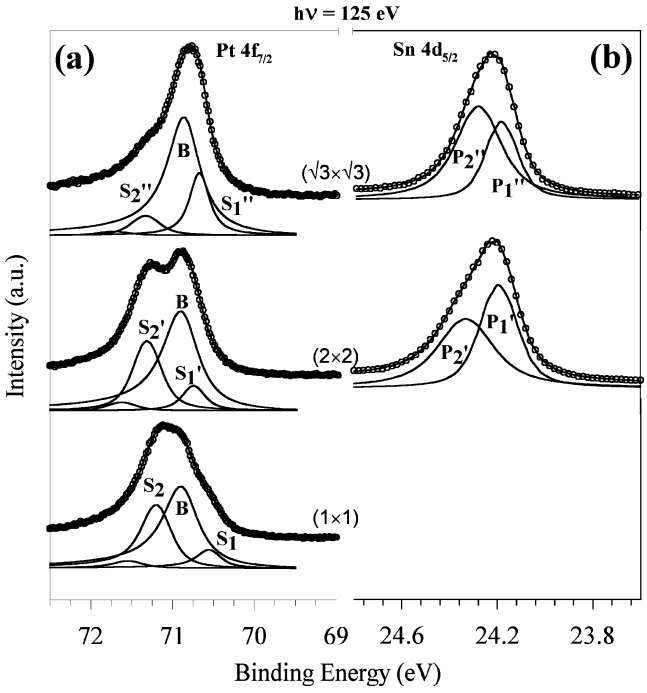

Fig. 3. (a) Core level spectra of Pt $4f_{7/2}$ and (b) Sn $4d_{5/2}$ recorded at 125 eV photon energy for Pt(111), Pt(111)Sn-(2 × 2), and Pt(111) Sn-($\sqrt{3} \times \sqrt{3}$)R30°, after exposure to 40 pulses of 2-butenal.

the ($\sqrt{3} \times \sqrt{3}$) surface alloys (S_1' and S_1'') shift slightly to higher binding energy, by 70 and 60 meV, as the 2-butenal dose increases. It is also worth noting that after 40 pulses, the relative intensities of S_2 and S_2' are more or less the same (33 and 32%), while the relative intensity of S_2'' is notably lower (9%). A summary of the intensities and surface shifts of the different components is given in Table 2. A fourth component, on the high binding energy side of the spectra, had to be added in order to get a good fit to the data, especially at high doses of 2-butenal. However, the binding energy of this component, as well as its intensity is not consistent throughout the experiment and can thus be induced by an unavoidable but negligible amount of surface defects or contaminants, detected due to the high surface sensitivity of our settings. The Sn $4d_{5/2}$ core-level spectra acquired on the (2 × 2) and the ($\sqrt{3} \times \sqrt{3}$) surface after exposure to 40 pulses 2-butenal are presented in Fig. 3b. The peak P_1' (P_1'') shifts slightly toward higher binding energy and a second component P_2' (P_2'') appears at 24.33 and 24.28 eV for (2 × 2) and ($\sqrt{3} \times \sqrt{3}$), respectively.

A clear influence of Sn on the adsorption of 2-butenal is seen in the C 1s core-level spectra. The main component in the C 1s spectrum at low coverage on the Pt(111) surface is labeled A in Fig. 4a, centered at 283.13 eV for 10 pulses. Some more complex features, on the high binding side, are also observed. Going from 10 to 20 pulses does

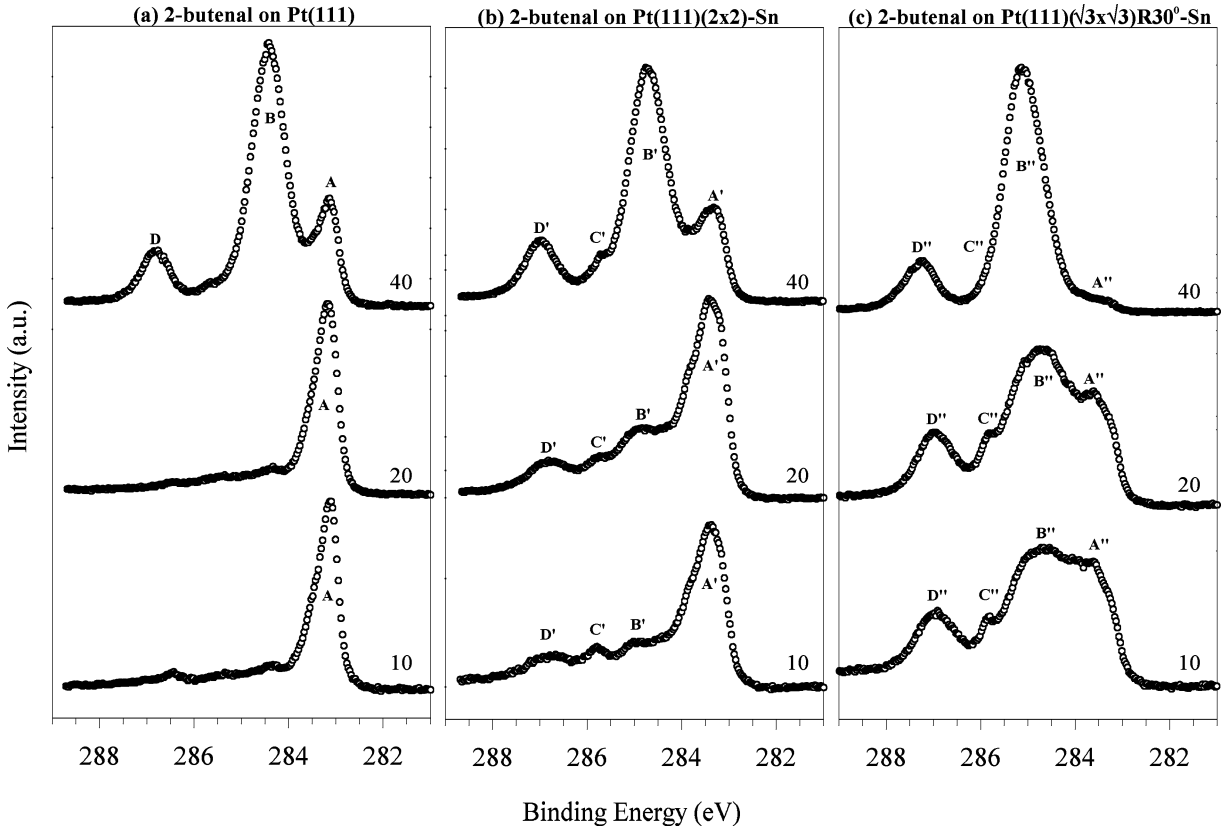

Fig. 4. (a) C 1s core-level spectra recorded at 374 eV photon energy after a 2-butenal dose of 10, 20, or 40 pulses on Pt(111), (b) Pt(111)Sn-(2 × 2), and (c) Pt(111)Sn-($\sqrt{3} \times \sqrt{3}$)R30°, respectively.

Table 3
Binding energies of the different components in the C 1s core level

2-Butenal		E_B			
Surface	Dose	A	B	C	D
(1 × 1)	10	283.13	–	–	–
	20	283.15	–	–	–
	40	283.12	284.41	–	286.81
(2 × 2)	10	283.34	284.60	285.81	286.70
	20	283.35	284.61	285.78	286.70
	40	283.35	284.73	285.74	286.99
($\sqrt{3} \times \sqrt{3}$)	10	283.38	284.67	285.83	286.95
	20	283.39	284.70	285.84	286.95
	40	283.42	285.12	–	287.28

not modify the binding energy of the main component nor its lineshape, but its intensity increases. At a 40-pulse exposure, two new components B and D appear in the spectrum at 284.41 and 286.81 eV, respectively. These peaks are broader than the A contribution. On the (2 × 2) surface, the main component in the C 1s spectrum at low coverage is labeled A′ in Fig. 4b, centered at 283.34 eV. This component is equivalent contribution A observed on the (1 × 1) surface. However, already at this low dose, three new components are discernible in the spectrum: B′ at 284.60 eV, C′ at 285.81 eV, and D′ at 286.70 eV binding energy. As was the case for the (1 × 1) surface, neither the binding energies nor the overall line shape of the C 1s spectrum are significantly changed when raising the 2-butenal dose to 20 pulses. Only the overall intensity increases. A 40-pulse exposure results in a drastic increase of the intensity of the B′ and D′ components. The behavior of the C 1s core level when 2-butenal is adsorbed on the ($\sqrt{3} \times \sqrt{3}$) surface alloy shares some similarities with the (2 × 2) spectrum. Four components appear at low coverage in the spectrum, labeled A″ at 283.38 eV, B″ at 284.67 eV, C″ at 285.83 eV, and D″ at 286.95 eV, as seen in Fig. 4c. The major difference, comparing the two tin-modified surfaces, lies in the relative intensities of the different contributions. Peak A″ is no longer the dominant component in the spectrum. Rather, peak B″ has the greater intensity, already at a 10-pulse coverage. Increasing the dose to 20 pulses does not significantly change the relative intensities of the different contributions. At 40 pulses, peaks B″ and D″ dominate the spectrum while peaks A″ and C″ are nearly unresolved. All binding energies are summarized in Table 3.

3. DFT calculations

3.1. Methods and models

Calculations with periodic boundary conditions have been performed using the DACAPO code [30]. The gradient-corrected PW91 exchange-correlation functional has been used [31]. Wave functions were expanded in terms of plane waves up to a kinetic energy of 340.145 eV. Core electrons were described by Vanderbilt ultrasoft pseudopotentials [32]. The Brillouin zone was sampled by 4 × 4 × 2 k-points [33]. Three different two-layer slabs were used as unit cells. For Pt(111), 18 Pt atoms were fixed at bulk positions. In the Pt(111)Sn-($\sqrt{3} \times \sqrt{3}$) surface alloy, tin atoms were fixed at positions 0.22 Å above the surface plane [17]. A somewhat smaller unit cell with 16 metal atoms was used for the Pt(111)Sn-(2 × 2) surface model. Here, the tin atoms were fixed 0.30 Å above the surface plane [17]. Surface adsorbates were allowed to relax, although surface atoms were kept rigid. The quality of the two-layer surface models was tested by comparing the adsorption energies for two equivalent adsorbate structures on two- and three-layer surface models. For a three-layer, 27 Pt slab, the adsorption energies changed only little, decreasing by 0.3 kcal/mol compared to (1 × 1)-**3** and by 0.9 kcal/mol compared to (1 × 1)-**5**. The two-layer surface models were thus accepted as being sufficiently accurate.

3.2. Results

The goal of the theoretical calculations has been to find the most favorable adsorption geometry of 2-butenal on Pt(111), Pt(111)Sn-(2 × 2), and Pt(111)Sn-($\sqrt{3} \times \sqrt{3}$), respectively, and correlate these results with the experimental observations. Fig. 5 gives schematic representations of the converged geometries [34]. The adsorption in structure **1** is dominated by a di-σ_{CC} bonding of the C–C double bond to a Pt pair. This type of C=C activation is known for shorter alkenes on Pt(111) and PtSn alloys [24,35–37]. In structures **2** and **3**, an additional bonding component is added as the carbonyl group rotates into position for an O–M bond [6]. Structure **4** represents a metalacycle geometry. The C_1–C_2 double bond present in this geometry displays a weak π-interaction with Pt. A simple O–M interaction is observed in structure **5**. The calculated energies of adsorption and selected geometrical parameters are presented in Tables 4 and 5. The intramolecular bond lengths of gas phase 2-butenal and 1-butenol are also given, as useful references.

The results show that a fairly large number of coordination geometries are possible for α,β-unsaturated aldehydes. On the clean Pt surface, (1 × 1)-**3** is the most stable structure. The carbon double bond of 2-butenal is clearly broken forming a di-σ_{CC} coordination to the metal. The O–Pt interaction elongates the carbonyl bond by 0.04 Å and shortens the C_1–C_2 bond by 0.05 Å, compared to (1 × 1)-**1**. Spectroscopic data for 2-butenal on Pt(111) agrees with a di-σ_{CC} coordination alongside a strong oxygen metal interaction [26]. On the tin-modified Pt(111)Sn-(2 × 2) surface, a similar 2-butenal coordination proves to be the most stable structure with the major difference that oxygen now coordinates to Sn ((2 × 2)-**3b**). Comparing the intramolecular distances of (1 × 1)-**3** and (2 × 2)-**3b** it is seen that the structures are very closely related. In the second most stable structure on the (2 × 2) surface, 2-butenal is bonded through a O–Sn in-

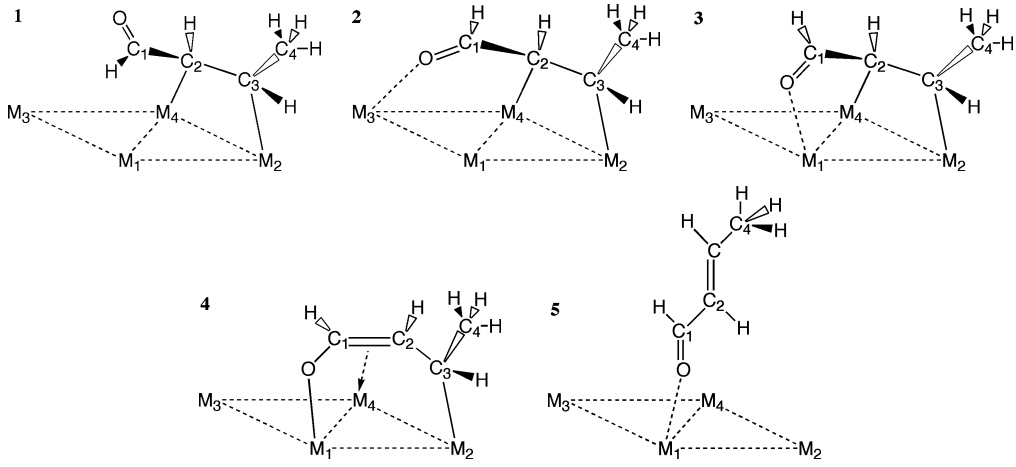

Fig. 5. Schematic representation of selected 2-butenal adsorption geometries.

Table 4
Adsorption energies (kcal/mol), calculated as the difference in energy between the adsorbed surface structures and the summed energy of gas-phase 2-butenal and clean surface

Entry	Site	ΔE_{ads}
(1×1)-**1**	$M_2 = M_4 = Pt$	−14.3
(1×1)-**2**	$M_2 = M_3 = M_4 = Pt$	−11.4
(1×1)-**3**	$M_1 = M_2 = M_4 = Pt$	−15.1
(1×1)-**4**	$M_1 = M_2 = Pt$	−8.5
(1×1)-**5**	$M_1 = Pt$	−5.5
(2×2)-**1**	$M_2 = M_4 = Pt$	0.0
(2×2)-**2**	$M_2 = M_4 = Pt$, $M_3 = Sn$	+0.3
(2×2)-**3a**	$M_1 = M_2 = M_4 = Pt$	+0.2
(2×2)-**3b**	$M_1 = Sn$, $M_2 = M_4 = Pt$	−8.5
(2×2)-**4**	$M_1 = Sn$, $M_2 = Pt$	−2.0
(2×2)-**5**	$M_1 = Sn$	−5.9
$(\sqrt{3} \times \sqrt{3})$-**1**	$M_2 = M_4 = Pt$	+4.0
$(\sqrt{3} \times \sqrt{3})$-**2**	$M_2 = M_3 = M_4 = Pt$	+12.0
$(\sqrt{3} \times \sqrt{3})$-**3**	$M_1 = Sn$, $M_2 = M_4 = Pt$	−1.1
$(\sqrt{3} \times \sqrt{3})$-**4**	$M_1 = Sn$, $M_2 = Pt$	+0.3
$(\sqrt{3} \times \sqrt{3})$-**5**	$M_1 = Sn$	−5.4

Table 5
Selected geometrical parameters of the investigated surface geometries (Å)

Entry	O–C_1	C_1–C_2	C_2–C_3	O–Sn	O–Pt	C_1–Pt	C_2–Pt	C_3–Pt
2-Butenal (g)	1.23	1.46	1.34	–	–	–	–	–
1-Butenol (g)	1.41	1.35	1.51	–	–	–	–	–
(1×1)-**1**	1.23	1.49	1.49	–	3.80	2.90	2.20	2.16
(1×1)-**2**	1.25	1.48	1.52	–	2.35	3.04	2.11	2.18
(1×1)-**3**	1.27	1.44	1.49	–	2.27	2.83	2.28	2.13
(1×1)-**4**	1.29	1.41	1.43	–	2.21	2.87	2.88	2.23
(1×1)-**5**	1.25	1.44	1.35	–	2.37	–	–	–
(2×2)-**1**	1.23	1.48	1.49	3.53	3.89	2.98	2.27	2.20
(2×2)-**2**	1.25	1.48	1.51	2.52	3.51	3.15	2.15	2.18
(2×2)-**3a**	1.26	1.45	1.49	3.08	2.68	2.96	2.32	2.19
(2×2)-**3b**	1.28	1.43	1.48	2.36	3.37	2.95	2.42	2.21
(2×2)-**4**	1.29	1.40	1.42	2.27	3.56	3.28	3.23	2.44
(2×2)-**5**	1.25	1.44	1.35	2.48	–	–	–	–
$(\sqrt{3} \times \sqrt{3})$-**1**	1.23	1.48	1.49	3.61	3.78	2.96	2.27	2.23
$(\sqrt{3} \times \sqrt{3})$-**2**	1.23	1.50	1.52	3.59	2.76	3.17	2.19	2.23
$(\sqrt{3} \times \sqrt{3})$-**3**	1.28	1.42	1.48	2.34	3.36	3.01	2.50	2.22
$(\sqrt{3} \times \sqrt{3})$-**4**	1.29	1.40	1.43	2.29	3.55	3.15	3.09	2.35
$(\sqrt{3} \times \sqrt{3})$-**5**	1.25	1.44	1.35	2.48	–	–	–	–

Heteroatom to metal distances refers to the closest surface atom.

teraction. A slight stretch of the carbonyl bond (0.02 Å) is observed for (2×2)-**5** compared to the free gas geometry. For Pt(111)Sn-$(\sqrt{3} \times \sqrt{3})$, $(\sqrt{3} \times \sqrt{3})$-**5** is the most stable structure, once again coordinating through a O–Sn bond.

It is clear that Sn generally weakens the interactions of 2-butenal with the platinum surfaces and this effect becomes more pronounced as the fraction of Sn increases in the surface alloy. This can be seen both by a general weakening of adsorption energies as well as from the increased bond lengths of similar structures, for instance comparing C–Pt bonds of (1×1)-**1**, (2×2)-**1**, and $(\sqrt{3} \times \sqrt{3})$-**1**, or (1×1)-**3**, (2×2)-**3b** and $(\sqrt{3} \times \sqrt{3})$-**3**. This is in agreement with experimental observations for various alkenes on these surfaces [23,24]. As will be commented upon below, the weakening of C–Pt interactions as Sn is introduced is also consistent with experimental data presented in this work.

4. Discussion

The adsorption of 2-butenal on the Pt(111) surface has previously been discussed in detail, where the participation of the carbonyl group in the bonding to the surface has been evidenced [26]. It should be noted that the calculations presented here predict an adsorption geometry given by (1×1)-**3**, being more stable than a geometry such as (1×1)-**2**, which has been suggested by others [6]. The component A was assigned to the vinylic (C_2–C_3–C_4) fragment of the molecule in (1×1)-**3**. The signal at B was attributed to the same molecular fragments, present in a multilayer phase, not interacting with the metal. Carbonyls in the multilayer phase resulted in D peaks. The absence of any contribution from the C=O group in the monolayer regime was attributed to the involvement of the oxygen atom in the bonding to the surface [26].

We will focus now on the influence of tin on the adsorption of the molecule. The C 1s line shape shows significant changes. Analogue with the assignment on the unmodified Pt(111) surface, the A′ and A″ components are attributed to the vinylic part of the molecule. These components are shifted by 0.20 eV (for A′) and 0.24 eV (for A″) compared to A, for a 20 pulse adsorbate dose. This shift is not attributed to a change in the adsorption mode, but rather to a weakening of the di-σ_{CC} bond strength, in agreement with calculations (see Table 5). The binding energy difference between the "surface-shifted" component S_1 and the "adsorbate-shifted" component S_2 in the Pt $4f_{7/2}$ core-levels spectra is practically the same for the three surfaces at low coverage. This indicates a retention of the di-σ_{CC} character of the bonding. A similar behavior has been reported for ethylene on these surfaces [38]. A new component appears in the low coverage spectra, labeled C′ for the (2×2), and C″ for the $(\sqrt{3} \times \sqrt{3})$ alloy. The binding energy difference observed between peaks A′ and C′ (A″ and C″) is equal to 2.43 eV (2.45 eV) at 20 pulses on the (2×2) ($(\sqrt{3} \times \sqrt{3})$) surfaces. A similar shift of 2.4 eV was found for propenal adsorbed on the Pt(111) surface at 95 K [39]. The high binding energy component was in this case assigned to the carbonyl group while the lower binding energy component was assigned to the vinylic part of the molecule. Consequently, the contributions C′ and C″ are attributed to the carbonyl carbon of 2-butenal molecule. It is interesting to note the early appearance of the B′ and D′ respective B″, D″ components when 2-butenal is adsorbed on the (2×2) and the $(\sqrt{3} \times \sqrt{3})$ surfaces. These components are analogue to peaks B and D, observed on the unmodified Pt(111) surface, which are assigned to a multilayer phase [26]. Furthermore, while A′ still dominates the C 1s spectrum (at low coverage) in the case of (2×2), B″, and D″ are the most intense peaks for $(\sqrt{3} \times \sqrt{3})$.

At this point we look closer at the correlation between the stable structures predicted by theory with the experimental results. As stated above, calculations predict (1×1)-**3**, (2×2)-**3b**, and $(\sqrt{3} \times \sqrt{3})$-**5** as the most stable adsorption geometries on the respective surfaces (see Table 4). At the lowest coverage, the C 1s spectra of the (1×1) and (2×2) systems show the same dominating component, namely A and A′, respectively. This is completely consistent with the preference for structure (1×1)-**3** and (2×2)-**3b**, i.e., 2-butenal structures with closely related geometries. For the $(\sqrt{3} \times \sqrt{3})$ surface, the components B″ and D″ are dominating already at 10 pulses of 2-butenal. Once again the most stable structure found by theory, i.e., $(\sqrt{3} \times \sqrt{3})$-**5**, is in agreement with this experimental finding, i.e., the presence of an important surface species with no carbon to surface interaction. The position of D″ suggests that the carbonyl is only weakly activated by the surface. The C 1s spectra indicate that more than one adsorption geometry may be present at the surface alloys. For (2×2), both B′ and D′ components are seen alongside A′ in the spectrum. This implies the additional presence of (2×2)-**5**, which is in fact the second most stable adsorption geometry according to calculations. For the $(\sqrt{3} \times \sqrt{3})$ surface the situation is reversed. Apart from the dominating components B″ and D″, a significant amount of A″ is also observed, implying that $(\sqrt{3} \times \sqrt{3})$-**3** coexists with $(\sqrt{3} \times \sqrt{3})$-**5**. These are the two most stable structures according to calculations (see Table 4). Returning to the C′ and C″ signals present in the spectra, we previously stated that these components were due to carbonyl carbons. It is not self-evident whether the carbonyl group interacts with the surface, as in variants of structure **3**, or if it is comparatively far from the surface, as in variants of structure **1**. Calculations predict very similar adsorbate structures for (1×1)-**3**, (2×2)-**3b** and $(\sqrt{3} \times \sqrt{3})$-**3**, with strong oxygen to surface interaction. Since the binding energy position of the C 1s carbonyl signal for the structure (1×1)-**3** has been proposed to overlap with the signal of the vinyl fragment (C_2–C_3–C_4) [26], we suggest that this is also the case for structures (2×2)-**3b** and $(\sqrt{3} \times \sqrt{3})$-**3**. Components C′ and C″ are of small intensity in all cases and could be due to minority species such as (2×2)-**1** and $(\sqrt{3} \times \sqrt{3})$-**1**.

The calculated structures also correlate well with other spectral data. Comparing the Pt $4f_{7/2}$ core-level spectra of the two surface alloys (see Fig. 3), it is clear that the adsorbate-induced peak decreases in intensity, going from the (2×2) to the $(\sqrt{3} \times \sqrt{3})$ alloy (S_2' vs S_2''). At the same time, the component due to clean platinum atoms at the surface increases (S_1' vs S_1''). This is consistent with the fact that Pt–adsorbate bonds are important on (2×2), while Sn–adsorbate bonds are important on $(\sqrt{3} \times \sqrt{3})$. The Sn $4d_{5/2}$ spectra of (2×2) and $(\sqrt{3} \times \sqrt{3})$ display two components for the 2-butenal-covered surfaces. Both peaks show shifts toward higher binding energies when comparing the clean and 2-butenal-covered surfaces, consistent with Sn taking part in the adsorbate bonding in both instances. It is not clear if the small energy shifts seen for P_1, 0.06 eV for (2×2) and 0.02 eV for $(\sqrt{3} \times \sqrt{3})$, are chemical shifts, i.e., if the two components in the spectra are indeed due to two different Sn–O interactions. However, O 1s spectra taken at the lowest and highest adsorbate coverages (10 and 40 pulses) show three components. A peak corresponding to carbonyl oxygen signal in the multilayer phase of 2-butenal is observed at 531.7 eV for (2×2) and at 532.0 eV for $(\sqrt{3} \times \sqrt{3})$. At lower binding energies, two overlapping peaks are observed at 530.0 and 531.3 eV for (2×2) and 530.1 and 531.6 eV for $(\sqrt{3} \times \sqrt{3})$. These results agree well with the idea of coexistence of different surface species, which calculations predict to be (2×2)-**3b** and (2×2)-**5** or $(\sqrt{3} \times \sqrt{3})$-**3** and $(\sqrt{3} \times \sqrt{3})$-**5**.

Insights into the influences of Sn on the selectivity in hydrogenation can be gained by comparing the trends and stable structures observed for the surfaces (1×1), (2×2), and $(\sqrt{3} \times \sqrt{3})$. It has been observed by us and by others that the addition of tin to platinum weakens the present C–Pt bonds [23,24]. As has been noted, we observe weakening of the adsorption energies and lengthening of the C–Pt

bonds on comparable structures, as the amount of Sn increases in the surface alloy (see Tables 4 and 5). Rodriguez et al. have proposed an electronic analysis of the Pt–Sn bond for PtSn(111)-($\sqrt{3} \times \sqrt{3}$)R30°, with a Sn(5s,5p) → Pt(6s,6p) charge transfer and a Pt(5d) → Pt(6s,6p) rehybridization [40]. The net result of the rearrangement is thus a decreased donor as well as acceptor ability of Pt. Tin, on the other hand, is more electrophilic after alloying with Pt and may therefore form bonds, e.g., with the free electron pairs of the carbonyl oxygen. In a sense, the introduction of the Pt surface with Sn therefore decreases the ability of the surface to activate the alkene bond of a α,β-unsaturated aldehydes, while the ability to activate the carbonyl bond is retained. This is illustrated in a pleasing and direct way by the most stable structures found for the two alloys investigated, i.e., (2 × 2)-**3b** and ($\sqrt{3} \times \sqrt{3}$)-**5**. In the former geometry 2-butenal is bound to the surface through a η_3(C,C,O) configuration, while in the latter only through a η_1(O) interaction. A preferential activation of the carbonyl bond no doubt points in the desired direction with respect to the original question of selectivity, i.e., forming the unsaturated alcohol of 2-butenal through hydrogenation. An important question is whether the activation of the carbonyl through Sn–O interaction is enough to enhance the carbonyl hydrogenation, compared to a Pt-only catalysts. In related work with supported Pt/Sn clusters it is often stated that tin in the form of Sn(II) or Sn(IV) is needed for improving selectivity toward unsaturated alcohol [41–43]. Recent experiments, where 2-butenal was hydrogenated over Pt/Sn surface alloys, did not show improved selectivity for 2-butanol [44]. Together with the results at hand, this suggests that the primary function of the Pt/Sn alloy is to impair the activation of the alkene bond, thereby affecting the hydrogenation selectivity. In this context, it is striking that a fairly small change in surface concentration of Sn, from 0.25 ML for (2 × 2) to 0.33 ML for ($\sqrt{3} \times \sqrt{3}$), can lead to a drastic shift in the structure of the surface species.

5. Conclusion

We have adsorbed 2-butenal (crotonaldehyde) on Pt(111) Sn-(2 × 2) and Pt(111)Sn-($\sqrt{3} \times \sqrt{3}$) surface alloys and compared the results with adsorptions on Pt(111). For Pt(111) we find 2-butenal adsorbed in a threefold hollow, with the alkene bonded in a di-σ_{CC} configuration and the carbonyl interacting with Pt through its oxygen lone pair. For the surface alloys, two surface species appear to coexist. One structure is analogue to the Pt(111) situation, i.e., a coordination in a threefold hollow, with the difference being that the carbonyl oxygen now coordinates to a tin atom. This structure dominates on Pt(111)Sn-(2 × 2) but a second surface species is also present, where 2-butenal coordinates to the surface only through a O–Sn interaction. On Pt(111)Sn-($\sqrt{3} \times \sqrt{3}$), this latter structure is the most stable. Upon increasing the Sn:Pt ratio, the carbonyl activation is thus retained while the alkene interaction with the surface is first weakened and later entirely eliminated.

Acknowledgments

This work was supported by the Swedish Research Council (VR). Parallelldatorcentrum (PDC) at the Royal Institute of Technology is gratefully acknowledged for providing computer facilities. H.v.S. would like to thank the Ernst Johnson Foundation for a grant. We thank Dr. Mats Nyberg for assistance with the DACAPO software and helpful discussions. The MAX-lab staff is acknowledged for its assistance.

References

[1] M. Bartok, K. Felföldi, Stereochemistry of Heterogeneous Metal Catalysis, Wiley, Chichester, 1985.
[2] R.L. Augustine, Heterogeneous Catalysis for the Synthetic Chemists, Dekker, New York, 1996.
[3] M. Bartok, A. Molnar, in: S. Patai (Ed.), Heterogeneous Catalytic Hydrogenations in Chemistry of Functional Groups, Wiley, New York, 1997, Supplement A3, The Chemistry of Double-Bonded Functional Groups.
[4] J. Jenck, J.E. Germain, J. Catal. 65 (1980) 141.
[5] P.N. Rylander, Catalytic Hydrogenation in Organic Syntheses, Academic Press, New York, 1979.
[6] F. Delbecq, P. Sautet, J. Catal. 152 (1996) 217.
[7] J.C. de Jesus, F. Zaera, Surf. Sci. 430 (1999) 99.
[8] J.L. Davis, M.A. Barteau, J. Mol. Catal. (1992) 109.
[9] C.-M. Pradier, Y. Berthier, G. Cordier, J. Oudar, Catalyst Deactivation, Elsevier, Amsterdam, 1991.
[10] C.-M. Pradier, T. Birchem, Y. Berthier, G. Cordier, Catal. Lett. 29 (1994) 371.
[11] T. Birchem, C.-M. Pradier, Y. Berthier, G. Cordier, J. Catal. 161 (1996) 68.
[12] S. Galvagno, Z. Poltarzewski, A. Donato, G. Neri, R. Pietropaolo, J. Chem. Soc. Chem. Commun. (1986) 1729.
[13] P. Beccat, J.C. Bertolini, Y. Gauthier, J. Massardier, P. Ruiz, J. Catal. 126 (1990) 451.
[14] M.T. Paffett, R.G. Windham, Surf. Sci. 208 (1989) 34.
[15] S.H. Overbury, D.R. Mullins, M.T. Paffett, Surf. Sci. 254 (1991) 45.
[16] S.H. Overbury, Y.-S. Ku, Phys. Rev. B 46 (1992) 7868.
[17] A. Atrei, U. Bardi, J.X. Wu, E. Zanazzi, G. Rovida, Surf. Sci. 290 (1993) 286.
[18] M. Gaoletti, A. Atrei, U. Bardi, G. Rovida, M. Torrini, Surf. Sci. 313 (1994) 349.
[19] E. Janin, H. von Schenck, S. Helldén, O. Tjernberg, U.O. Karlsson, M. Göthelid, Surf. Sci., in press.
[20] M.T. Paffett, S.C. Gebhard, R.G. Windham, B.E. Koel, J. Phys. Chem. 94 (1990) 6831.
[21] C. Xu, B.E. Koel, Surf. Sci. Lett. 304 (1994) L505.
[22] E. Janin, M. Björkqvist, T.M. Grehk, M. Göthelid, C.-M. Pradier, U.O. Karlsson, A. Rosengren, Appl. Surf. Sci. 99 (1996) 371.
[23] Y.-L. Tsai, C. Xu, B.E. Koel, Surf. Sci. 385 (1997) 37.
[24] Y.-L. Tsai, B.E. Koel, J. Phys. Chem. B 101 (1997) 2895.
[25] C. Panja, N. Saliba, B.E. Koel, Surf. Sci. 395 (1998) 248.
[26] E. Janin, S. Ringler, J. Weissenrieder, T. Åkermark, U.O. Karlsson, M. Göthelid, Surf. Sci. 482–485 (2001) 83.
[27] R. Denecke, Väterlein, P.M. Bässler, N. Wassdahl, Butorin, S.A. Nilsson, J.-E. Rubensson, J. Nordgren, N. Mårtensson, R. Nyholm, J. Electron. Spectrosc. Relat. Phenom. 101–103 (1999) 971.

[28] N. Mårtensson, P. Baltzer, P. Brühwiler, J.-O. Forsell, A. Nilsson, A. Stenborg, B. Wannberg, J. Electron. Spectrosc. Relat. Phenom. 70 (1994) 117.
[29] See O. Björneholm, A. Nilsson, H. Tillborg, P. Bennich, A. Sandell, B. Hernnäs, C. Puglia, N. Mårtensson, Surf. Sci. 315 (1994) L983, and references therein.
[30] DaCapo is a free pseudopotential plane-wave based DFT code available at http://www.fysik.dtu.dk/CAMPOS/ developed and distributed by CAMP (Center for Atomic-Scale Materials Physics).
[31] J.P. Perdew, J.A. Chevary, S.H. Vosko, K.A. Jackson, M.R. Pederson, D.J. Singh, C. Fiolhaism, Phys. Rev. B 46 (1992) 6671.
[32] D. Vanderbilt, Phys. Rev. B 41 (1990) 7892.
[33] H.J. Monkhorst, J.D. Pack, Phys. Rev. B 13 (1976) 5188.
[34] Starting geometries (2×2)-**5** and $(\sqrt{3} \times \sqrt{3})$-**5** with $M_1 = Pt$, as well as (2×2)-**4** and $(\sqrt{3} \times \sqrt{3})$-**4** with M_1, $M_2 = Pt$, converged to approximately free 2-butenal gas at the surface with O–Pt distances around 3 Å. Starting geometries, with 2-butenal bonded to a Pt pair through a di-σ_{CO} bond on (1×1) converged into (1×1)-**5**. Starting geometries with 2-butenal bonded to a Pt–Sn pair through a di-σ_{CO} bond on (2×2) and $(\sqrt{3} \times \sqrt{3})$, converged into (2×2)-**5** and $(\sqrt{3} \times \sqrt{3})$-**5**, respectively.
[35] M. Salmeron, G.A. Somorjai, J. Phys. Chem. 86 (1982) 341.
[36] R.J. Koestner, J.C. Frost, P.C. Stair, M.A. Van Hove, G.A. Somorjai, Surf. Sci. 116 (1982) 85.
[37] N.R. Avery, N. Sheppard, Proc. Roy. Soc. London A 405 (1986) 1.
[38] M.T. Paffett, S.C. Gebhard, R.G. Windham, B.E. Koel, Surf. Sci. 223 (1989) 449.
[39] F. Bournel, C. Laffon, Ph. Parent, G. Tourillon, Surf. Sci. 350 (1996) 78.
[40] J.A. Rodriguez, S. Chaturvedi, T. Jirsak, J. Hrbek, J. Chem. Phys. 109 (1998) 4052.
[41] J.L. Margitfavli, A. Tompos, I. Kolosova, J. Valyon, J. Catal. 174 (1998) 246.
[42] J.L. Margitfavli, G. Vanko, I. Borbath, A. Tompos, A. Vertes, J. Catal. 190 (2000) 474.
[43] V. Ponec, Appl. Catal. A 149 (1997) 27, and references cited therein.
[44] D.M. Jerdev, A. Olivas, B.E. Koel, J. Catal. 205 (2002) 278.